scientific reports

OPEN

One-pot synthesis of zinc oxide nanoparticles via chemical precipitation for bromophenol blue adsorption and the antifungal activity against filamentous fungi

Kovo G. Akpomie[1,2✉], Soumya Ghosh[3], Marieka Gryzenhout[3] & Jeanet Conradie[1]

In this research, zinc oxide nanoparticles (ZnONPs) were prepared via a facile one-pot chemical precipitation approach and applied in the adsorption of bromophenol blue (BRB) and as antifungal agents against the filamentous fungi and plant pathogens; *Alternaria alternata* CGJM3078, *Alternaria alternata* CGJM3006 and *Fusarium verticilliodes* CGJM3823. The ZnONPs were characterized by the UV–Vis, FTIR, XRD, TGA, BET, SEM, TEM, and EDX techniques, which showed efficient synthesis. The characteristics ZnO UV–Vis absorption band was observed at 375 nm, while the XRD showed an average ZnONPs crystalline size of 47.2 nm. The SEM and TEM images showed an irregular shaped and aggregated porous structure of 65.3 nm average-sized ZnONPs. The TGA showed 22.9% weight loss at 800 °C indicating the high thermal stability of ZnONPs, while BET analysis revealed a surface area, pore volume and pore diameter of 9.259 m^2/g, 0.03745 cm^3/g and 9.87 nm respectively. The Freundlich, pseudo-second-order, and intra-particle diffusion models showed R^2 > 0.9494 and SSE < 0.7412, thus, exhibited the best fit to the isotherm and kinetics models. Thermodynamics revealed feasible, endothermic, random, and spontaneous adsorption of BRB onto the synthesized ZnONPs. The antifungal assay conducted depicts strong antifungal activities against all three tested fungi. Noticeably, ZnONPs (0.002–5 mg/mL) showed maximum activities with the largest zone of inhibition against *A. alternata* CGJM 3006 from 25.09 to 36.28 mm. This was followed by the strain *F. verticilliodes* CGJM 3823 (range from 23.77 to 34.77 mm) > *A. alternata* CGJM3078 (range from 22.73 to 30.63 mm) in comparison to Bleach 5% (positive control). Additionally a model was proposed based on the possible underlying mechanisms for the antifungal effect. This research demonstrated the potent use of ZnONPs for the adsorption of BRB and as effective antifungal agents.

In recent years, there have been growing concerns arising from the rapid pollution of water bodies around the world[1]. This is attributed to technological advancements resulting in the rapid growth of industries, and subsequently the pollution of water from industrial effluents[2,3]. This water pollution has significantly affected aquatic lives, made the water unsafe for drinking, and resulted in several health effects[4,5]. Among several water pollutants, dyes have gained significant attention from environmental scientists[6]. This is because dyes are extensively used in the textile, leather, cosmetic, and paper industries[7]. The textile industry alone consumes over 700,000 tons of dyes annually[8,9]. Thus, there is a high amount of dyes in the effluents released from these industries. Apart from that, dyes are allergenic, mutagenic, and carcinogenic at certain concentrations, hazardous, affect photosynthesis in marine organisms, and are resistant to biodegradation[10]. Therefore, the treatment of dye-polluted water is important.

Bromophenol blue (BRB) dye is widely used as a laboratory indicator and in the textile and printing industries[8,11]. However, most studies have focused on the treatment of water contaminated with dyes such as methylene blue, congo red, and malachite green, but only a few studies are documented the removal of BRB despite its harmful nature in the environment[12]. Hence, this research considers the removal of BRB from water.

[1]Department of Chemistry, University of the Free State, Bloemfontein, South Africa. [2]Department of Pure & Industrial Chemistry, University of Nigeria, Nsukka, Nigeria. [3]Department of Genetics, University of the Free State, Bloemfontein ZA9300, South Africa. ✉email: kovo.akpomie@unn.edu.ng

Several methods have been utilized over the years for the treatment of dye-polluted water such as filtration, coagulation, solvent extraction, precipitation, adsorption, ion exchange, floatation, biological treatment, catalytic degradation, ozonation, and oxidation[13,14]. Adsorption is the most efficient and promising method but is limited by the high cost of activated carbon used as a commercial adsorbent for water treatment[9,15]. Therefore, other efficient low-cost adsorbents such as bio-waste, natural inorganic materials, polymeric materials, and nanomaterials have been harnessed as suitable alternatives to activated carbon[10,16–21].

Among the alternative adsorbents, nanomaterials have gained tremendous attention in recent years due to their high efficiency, high surface reactivity, broad application for several purposes, and environmental compatibility[8,17,22]. Metallic nanoparticles are known to be promising owing to their efficient adsorptive and catalytic degradation potentials for dye containing water[23–25]. In particular, zinc oxide nanoparticles (ZnONPs) have received significant attention for water treatment because of their nontoxicity, long-term stability, acceptable cost, biocompatibility, surface properties and potent antimicrobial activities against microbes frequently encountered in water[26–28]. Thus, a combination of the adsorption potentials and the antimicrobial activities in water treatment would be highly effective to obtain portable water. Therefore, the efficient treatment of dye-polluted water by the use of ZnONPs is well documented[26,29,30]. However, from a thorough literature search, there is no evidence of the use of ZnONPs in the adsorption of BRB from water. Thus, this study evaluated for the first time the potentials of ZnONPs in the treatment of BRB polluted water.

Several studies have been performed on the antibacterial and antifungal activities of ZnONPs, which proved that ZnONPs are potent antimicrobial agent[27,31–35]. However, studies on the antifungal activity of nanoparticles against filamentous fungi are rare[36,37]. In this study, the two plant pathogens were studied. The filamentous fungus *Alternaria alternata* is a pathogen of fruit and vegetables such as strawberries, tangerines, mandarins, grapefruits, and tomatoes, thus causing extensive post-harvest spoilage and loss[38,39]. Additionally, *A. alternata* employs cell wall degrading enzymes, such as pectic enzymes, and organic acids that lower the pH and act synergistically with the enzymes to digest calcium-acetate, which causes damage to the host tissues[38]. In humans, *Alternaria alternata* is associated with hypersensitivity pneumonitis, bronchial asthma, allergic sinusitis, rhinitis, and cutaneous, subcutaneous infections in humans[40].

The filamentous fungus *Fusarium verticilliodes* is a seed-borne endophytic pathogen of maize and cereals such as wheat, and can infect a wide variety of other plants worldwide[41,42]. Besides, *F. verticilliodes* secretes fumonisin B that accumulates in the kernels of maize or wheat, causing toxicity in resulting food commodities[43,44]. *Fusarium* mycotoxin adulteration in agricultural commodities poses a global threat to food safety and has substantial economic significances[45,46].

There is a need to discover novel control agents to prevent plant diseases and post-harvest losses of food crops and grains associated with filamentous fungi, as well as to minimize harmful effects of these fungi on humans and livestock. Although a few studies have reported ZnONPs antifungal activities against *Alternaria alternata*[36,37], no study was conducted specifically on the two strains (CGJM3078 and CGJM3006) of *Alternaria alternata*. Besides, no antifungal studies with ZnONPs were conducted so far against strains of *F. verticilliodes*. The present study investigated the extent of the antifungal activities of ZnONPs against these economically significant postharvest fungal pathogens.

The aim of this study is the evaluation of the adsorptive potentials of ZnONPs for BRB dye as well as the antifungal activity against *A. alternata* and *F. verticilliodes*. The ZnONPs were synthesized by a simple traditional one-pot chemical precipitation approach and characterized. The synthesized ZnONPs were then utilized for BRB adsorption. Finally, the antifungal activity of the synthesized ZnONPs against *A. alternata* and *F. verticilliodes* was investigated in vitro, and a possible mechanism of action against these fungi was proposed.

Materials and methods

Chemicals used. Zinc acetate dihydrate ($Zn(CH_3COO)_2 \cdot 2H_2O$), bromophenol blue ($C_{19}H_{10}Br_4O_5S$), sodium hydroxide (NaOH), nitric acid (HNO_3), and hydrochloric acid (HCl) were purchased from Sigma-Aldrich, South Africa. All the chemicals were used as purchased without any purification.

Synthesis of ZnONP. A simple one-pot synthesis via chemical precipitation was utilized for the preparation of ZnONPs[47]. Herein, 4.0 g of zinc acetate was added to 100 mL of distilled water in a beaker. The solution was stirred with a magnetic stirrer on a hot plate at 30 °C for 40 min. This was followed by the dropwise addition of 0.2 M NaOH to the solution with continuous stirring until the pH was 11.0. The solution became white due to the precipitation of ZnO and $Zn(OH)_2$, the solution was stirred further for 1 h, after which it was allowed to stand for 50 min. The filtrate was decanted and the synthesized precipitate was washed repeatedly with excess distilled water until neutral pH and finally with ethanol. The precipitate was further dried in an oven at 250 °C for 5 h in order to decompose any $Zn(OH)_2$ into ZnONPs. The as-prepared ZnONPs were stored in an airtight sample container and kept in a desiccator until use.

Characterization of the synthesized ZnONPs. The ZnONPs were characterized to evaluate the surface properties necessary for efficient adsorption of BRB from water. The field emission scanning electron microscopy (FE-SEM; Jeol model) was used to examine the particle size and morphology, while the Energy-dispersive X-ray spectroscopy (EDS; Oxford model) coupled to the SEM instrument was used to determine the elemental composition. The morphology and surface structure was further analyzed with the Transmission electron microscopy (TEM) (Philips-FEI-CM100 model) equipped with a Mega View III digital camera. The functional groups of ZnONP were examined by the Fourier transform infrared (FTIR) spectroscopy (FTIR; Bruker Tensor 27 model). The crystalline phases were identified by the X-ray diffractometer (XRD; Brucker model) with Cu radiation of 1.5 Å at the 2-theta range of 10°–80°. The pH drift method was used to evaluate the pH point of

Parameters	Range studied	Conditions maintained
Solution pH	2, 3, 4, 5, 6, 7, 8, 9	Dosage 0.1 g, dye conc 50 mg/L, time 180 min, temp 300 K
ZnONP dosage (g)	0.1, 0.15, 0.2, 0.25, 0.3	pH 4.0, dye conc 50 mg/L, time 180 min, temp 300 K
Dye concentration (mg/L)	10, 20, 30, 40, 50	pH 4.0, dosage 0.1 g, time 180 min, temp 300 K
Sonication time (min)	5, 10, 20, 40, 60, 80, 100, 120, 140, 160, 180	pH 4.0, dosage 0.1 g, dye conc 50 mg/L, temp 300 K
Temperature (K)	300, 306, 313, 318, 323	pH 4.0, dosage 0.1 g, dye conc 50 mg/L, time 180 min

Table 1. Effect of various parameters and operating conditions on the adsorption of bromophenol blue onto ZnONPs.

zero charge (pHpzc) as described elsewhere[48]. The UV absorption spectra of the ZnONPs were obtained using distilled water as a reference with the UV-Spectrophotometer (Shimadzu UV-1800 model) in the range 250 to 850 nm. Thermal stability was analyzed by the thermo-gravimetric analyzer (TGA; Mettler Toledo Model). The surface area analyzer (Micrometrics ASAP 2020 model) was used to examine the Surface area (S_{BET}) and pore properties and the results were refined by the MicroActive VI.01 software.

Adsorption removal. A stock solution of BRB was made by dissolving 50 mg of $C_{19}H_{10}Br_4O_5S$ in a 500 mL volumetric flask to make a concentration of 100 mg/L. Serial dilution of the stock was done to obtain lower concentrations of 10–50 mg/L. The pH of the solution was adjusted from 2.0 to 9.0 using 0.1 M NaOH and HCl. Batch adsorption was applied to determine the influence of solution pH, ZnONPs dosage, BRB concentration, sonication time, and temperature at the operating conditions presented in Table 1. Batch BRB adsorption was carried out by adding a given amount of ZnONPs to 10 mL of a given BRB concentration at the specified pH. The mixture was sonicated at a particular temperature in an ultrasonic 2.5 L water-filled bath at the specified time. At the end of the given time, the solution was centrifuged at 8000 rpm for 30 min, and the filtrate was analyzed for residual BRB at a maximum wavelength of 590 nm, using the UV spectrophotometer (Shimadzu UV-1800 model). The percentage adsorption and uptake capacity q_e (mg/g) were calculated from the percentage removal and mass balance equations, respectively[8]:

$$Adsorption(\%) = \left(\frac{(C_o - C_e)}{C_o} \right) * 100 \tag{1}$$

$$q_e = \frac{(C_o - C_e)V}{m} \tag{2}$$

where C_e and C_o in mg/L are the final and initial concentrations of BRB in solution, respectively. m (g) is the mass of ZnONPs used and V (L) is the volume of BRB solution used.

Isotherm, kinetic and thermodynamics of adsorption. The isotherm modeling on the adsorption of BRB onto ZnONPs was evaluated from the Freundlich, Temkin, Langmuir, and Flory–Huggins models [12]. The adsorption kinetics was deduced from the pseudo-first-order (PFO), pseudo-second-order (PSO), liquid film diffusion (LFD), and intraparticle diffusion (IPD) rate models, while thermodynamics was deduced from Van't Hoff's Equation [49]. The equation and symbols of the isotherm, kinetics, and thermodynamics are described in the Supplementary Information.

Statistical analysis. Each experiment was done in duplicate and the average value was computed. The error bars in the figures indicate the standard deviation from the mean. The statistical function of the origin 2019b software was used to determine the sum square error (SSE) and the coefficient of determination (R^2), used to analyze the best-fitted isotherm or kinetic model.

Antifungal analysis. The in vitro antimicrobial activities of the ZnONPs were tested against the three fungal strains, viz *A. alternata* CGJM3078, *A. alternata* CGJM3006, and *F verticilliodes* CGJM3823 fungi [CGJM = Cultures Gert Johannes Marais]. The fungal strains were procured from Dr. Gert Marais, Department of Plant Sciences, University of the Free State, Bloemfontein, South Africa. The antimicrobial activity screening was performed with the well diffusion technique[50,51] on malt agar (Malt extract 2%; Dextrose 2%; Agar 2% Biolab, Merck, Johannesburg) media plates. For the technique, a pinch amount of mycelia scraping from each of the fungi was inoculated in 15 mL of Malt extract dextrose broth (Malt extract 2%; Dextrose 2%) and cultivated for 3 days at 25 °C. Following the incubation, the cultures were adjusted to a concentration of 10^6 cfu/mL (cfu—colony forming units), inoculated in molten Malt Extract Agar, swirled gently, and poured into 90 mm Petri plates (Ascendis, Johannesburg). The inoculated plates were dried under a Bio-Safety Cabinet Class II (ESCO Technologies Pty Ltd, Gauteng, South Africa).

Following air-drying, the solidified agar media plates were bored (bore size = 5 mm) with wells with a metallic plug borer and filled with 40 μL of the ZnONPs made into twofold serial dilutions (0.002, 0.004, 0.009, 0.019, 0.039, 0.078, 0.156, 0.312, 0.625, 1.25, 2.5, 5) mg/mL, in accordance to a previous study[33]. Bleach disinfectant [Ca(ClO)$_2$] (5%) served as the positive control while sterile distilled water was used as the negative control for

all the experiments. Plates were incubated at room temperature in the upright position until zones of inhibition were observed, which was considered an endpoint parameter for the antimicrobial activities. The diameter of the inhibition zones was measured using the Image J software program (https://imagej.nih.gov/ij/) as per a previous study[51]. All the culture media were procured from Sigma Aldrich, Merck KGaA, Darmstadt, Germany, and Neogen Culture media, Heywood, UK respectively.

Results and discussion

Characterization of ZnONP. The XRD characterization used to examine the crystalline phases of ZnONPs is shown in Fig. 1a. The spectrum showed diffractions patterns at 2θ values of 31.69°, 34.33°, 36.11°, 47.43°, 56.49°, 62.76°, 66.23°, 67.88°, 68.97°, 72.37° and 76.93°, which conforms to the hexagonal ZnO crystalline planes of (100), (002), (101), (102), (110), (103), (200), (112), (201), (004) and (202) respectively, as indexed in the standard JCPDS card no. 36-1451[26]. This confirms the successful synthesis of ZnO. The XRD result is similar to that reported in the green synthesis of ZnONPs using the extract of stevia[52]. In addition, the as-prepared ZnONPs had high crystalline structure as revealed by the high intensity of the diffraction peaks. Apart from that, the fact that no other diffraction peak was observed in the XRD suggests pure synthesized ZnONPs. The average nanoparticle crystalline size of ZnONPs as deduced from the Debye–Scherrer's equation was 47.2 nm using the characteristic peak at 36.11°. This is similar to the ZnONPs sizes in the range of 40.3–49.3 nm obtained from the biosynthesis using the extract of *Prosopis farcta* at different concentrations of the precursor ($ZnSO_4 \cdot 7H_2O$)[53]. Besides, the size was larger than 15.41 nm and 5–15 nm reported in the green synthesis of ZnONPs using aqueous extracts of *Deverra tortuosa*[54] and *Mussaenda frondsa*[55] respectively.

The FTIR spectra of ZnONPs before and after the adsorption of BRB are shown in Fig. 1b. The spectra help to identify the functional groups present on ZnONPs. The band at 3369 cm^{-1} corresponds to the O–H stretching vibration, while the O=C=O functionality of absorbed CO_2 on the ZnONPs was depicted by the bands at 2162 cm^{-1} and 2008 cm^{-1}[56]. The absorption band at 1380 cm^{-1} corresponds to the OH bending of water acquire from the absorption of moisture from air[26]. Also, the Zn–O stretching vibrations were indicated by the bands at 887 cm^{-1} and 550 cm^{-1}, which confirms the successful synthesis of the ZnONPs. After the adsorption of dye, the BRB-loaded ZnONPs showed shifts in absorption bands from 3369 to 3377 cm^{-1} and 1380 to 1330 cm^{-1} for OH, from 2008 to 2033 cm^{-1} for the O=C=O, and from 550 to 557 cm^{-1} for the Zn–O functionalities. This indicated the involvement of the OH and Zn–O groups in the uptake of BRB on the adsorbent and that the mechanism of BRB uptake on ZnONPs could be attributed to electrostatic interactions, H-bonding as well as weak Vander Waals interaction[47].

The UV spectrum of the as-prepared ZnONPs is shown in Fig. 1c. The characteristic ZnO peak was observed at 375 nm, this corroborates the efficient and successful synthesis of ZnONPs. The absorption at 375 nm is attributed to the intrinsic bandgap of ZnO from the valence to the conduction bands resulting from the electronic transitions[57]. Similar UV absorption was achieved at 374 nm for the green synthesis of ZnONPs using the aqueous extract of *Deverra tortuosa*[54]. Also, Zare et al.[58] showed a similar UV absorption of green synthesized ZnONPs in the range of 376–360 nm, while absorptions at 350–370 nm was reported by Khatami et al.[59]. The thermal stability of the synthesized ZnONPs was evaluated from the TGA as presented in Fig. 1d. Significant weight loss was observed from 98 to 206 °C, which could be attributed to the removal of absorbed water, CO_2 as well as other low-temperature components from the synthesized ZnONPs. At 800 °C, the ZnONPs showed a weight loss of 22.92% indicating high thermal stability of 78.98%. The as-prepared ZnONPs demonstrated efficient thermal stability in comparison to that prepared by Yuvaraja et al.[29], which showed over 35% weight loss up to 450 °C. This indicated the efficiency of our synthetic procedure in the preparation of ZnONPs with enhanced thermal characteristics for higher temperature applications.

The nitrogen adsorption–desorption isotherm (Fig. 1e) of the ZnONPs as obtained from BET analysis revealed a surface area of 9.259 m^2/g and correlated with type III isotherm according to the IUPAC classification[47]. Also, the pore characteristics (Fig. 1f) as obtained from the Barret-Joyner-Halenda (BJH) method showed a pore volume of 0.037453 cm^3/g and an average pore diameter of 9.87 nm indicating the mesoporous structure. Although the surface area of our as-prepared adsorbent was lower than 26.78 m^2/g obtained from the hydrothermal synthesis of ZnONPs used in the adsorption of heavy metals[26], the mesoporous structure (see discussion in the next paragraph) would be highly influential for the efficient removal of dye molecules from solution[60].

The SEM images of the as-prepared ZnONPs are shown in Fig. 2a and b. As observed, the ZnONPs adsorbent is associated with an irregular surface structure, particle aggregation, with a highly porous morphology, which corroborates the porosity measurements. The average ZnONPs size of 65.3 nm was obtained from the SEM structure. This lies in the size range of 60–72 nm obtained in the hydrothermal synthesis of ZnONPs[61]. Again, the porous structure of the synthesized ZnONPs would ensure easy diffusion of dyes molecules favoring efficient adsorption of the pollutant from solution[62]. The agglomerated characteristics of the synthesized ZnONPs were further verified from the TEM image (Fig. 2c). Besides, the EDX spectra (Fig. 2d) of the adsorbent, showed 78.9% zinc and 21.1% oxygen, which further confirms the successful synthesis of the ZnONPs. The absence of other elements also indicates a pure synthesized ZnONPs, which corroborated the results of the XRD analysis. A similar finding was also reported by other workers[26,63,64]. The absence of impurities in the synthesized ZnONPs is important for efficient antimicrobial activity[64].

BRB uptake on ZnONPs. Several operating parameters such as the temperature of the solution, dye concentration, solution pH, time, and material dosage are known to influence the overall uptake of pollutants onto adsorbent materials[17,65,66]. Thus, we investigated the effect of these parameters on the uptake of BRB onto ZnONPs. Figure 3a illustrates the influence of pH on dye removal from solution onto the as-prepared particle. A steady decrease in the adsorbent's adsorption capacity and percentage uptake of BRB from pH 2.0 to 6.0 was
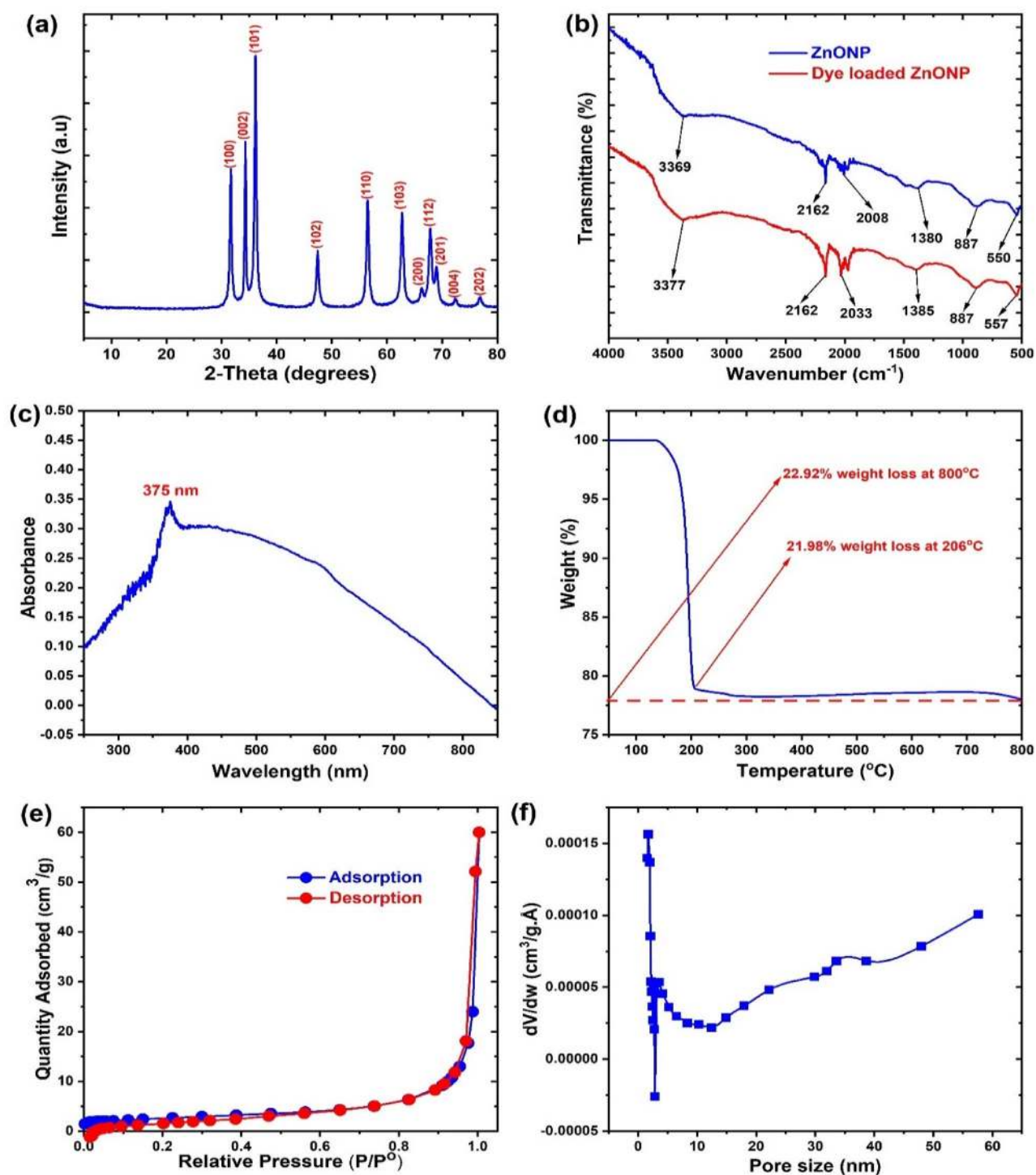
Figure 1. The (**a**) X-ray diffraction (**b**) Fourier transform infrared (**c**) Ultraviolent spectra (**d**) Thermogravimetric analysis (**e**) Nitrogen adsorption–desorption isotherm and (**f**) Pore analysis of the synthesized ZnONPs.

obtained after which a slight increase up to pH 9.0 was observed. This trend is strongly dependent on the pHpzc of ZnONPs as well as the pKa of BRB dye in solution. The pHpzc is the pH at which the net surface charge on the adsorbent is zero[67]. Usually the adsorbent surface is positively or negatively charged at pH values below and above the pHpzc, respectively[68]. The pHpzc of the synthesized ZnONPs was 6.3 while BRB has a pKa value of 3.84[8]. Thus, ZnONPs are associated with a positive surface charge at pH values below 6.3 but becomes negative above this pH. Also, BRB exists as negatively charged molecules below 3.84 after which it becomes neutral and then exists as positively charged species as pH increases. Thus the optimum uptake achieved at pH values below
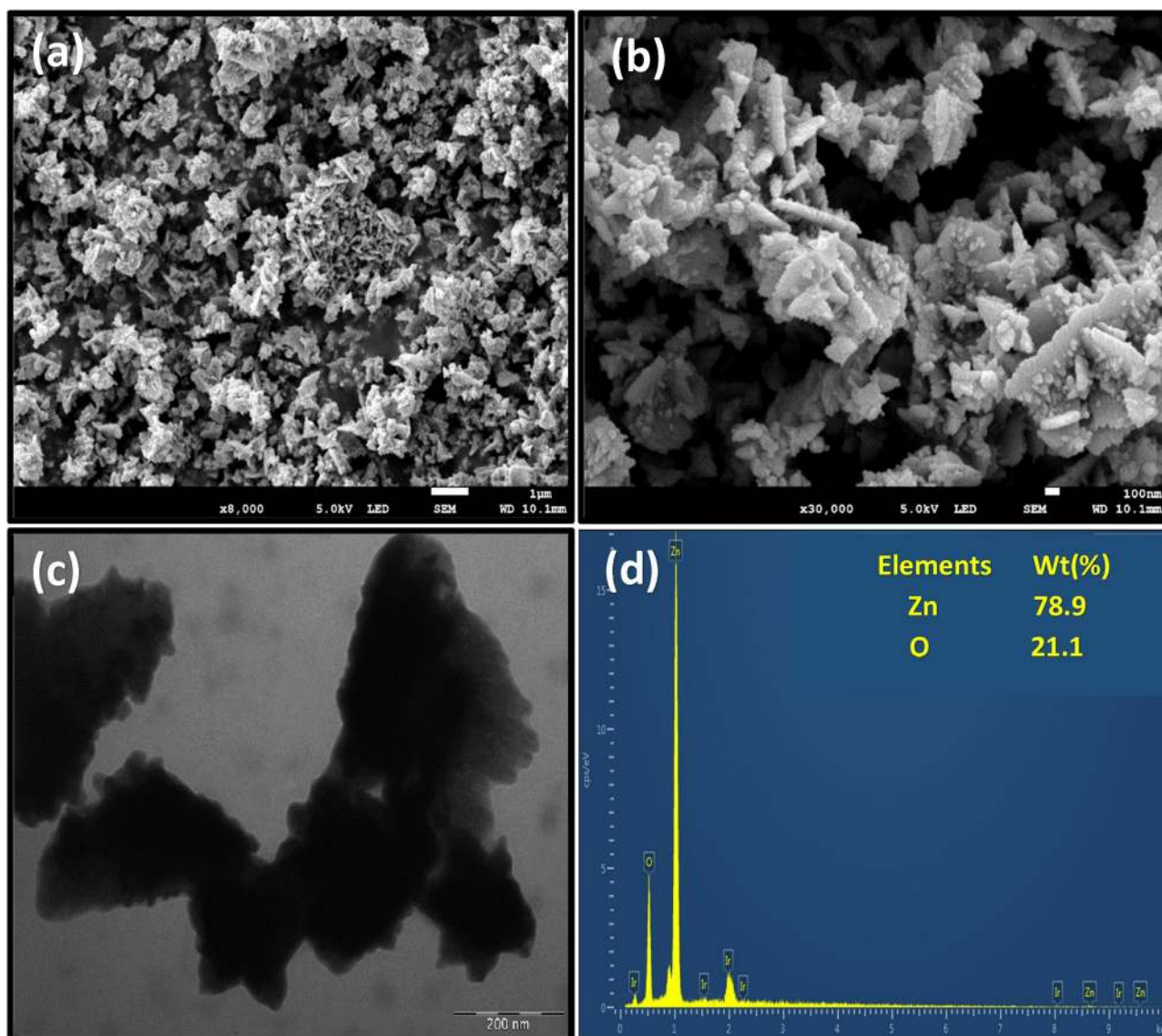
Figure 2. The (**a**, **b**) Scanning Electron microscopy (**c**) Transmission electron microscopy and (**d**) Energy dispersive X-ray spectrum of the synthesized ZnONPs.

4.0 was due to strong electrostatic attraction between the positive ZnONPs surfaces and the anionic BRB species in solution. Again, the slight increase observed from pH 6.0 to 9.0 is probably due to the attraction between positively charged BRB species in solution and the negatively charged adsorbent surface. Although optimum BRB removal was obtained at pH 2.0, this pH is too acidic to be associated with real dye-polluted wastewaters. Therefore, we selected pH 4.0 for subsequent experiments due to its closer association with real dye polluted water and the higher uptake recorded compared to values from pH 5.0 to 9.0.

The influence of the initial concentration of dye on the removal of BRB onto ZnONPs is shown in Fig. 3b. With the increase in BRB concentration from 10 to 50 mg/L, an increase in the adsorption capacity of ZnONPs from 0.82 to 2.53 mg/g and a decrease in percentage adsorption from 82.1 to 50.6% was displayed. This trend is consistent with the findings of other researchers[26,69,70]. Thus as the BRB concentration in the aqueous phase increased, more BRB molecules were fixed on the active sites of ZnONPs[71], which resulted in site saturation, surface repulsions, and less percentage removal of dye from solution[72]. The BRB concentration of 50 mg/L was selected for the batch experiments due to the associated optimum adsorption capacity, which indicated effective utilization of the actives sites of the as-prepared ZnONPs. On the other hand, the effect of ZnONPs dosage on the removal of BRB on the adsorbent displayed an opposite trend to that of the initial dye concentration. As observed from Fig. 3c, with increasing dosage of ZnONPs from 0.1 to 0.3 g, a decrease in the adsorption capacity from 2.53 to 1.17 mg/g and an increase in the percentage adsorption of BRB from 50.6 to 70.2% was recorded. Since the BRB concentration in solution was constant at 50 mg/L, as the dosage of ZnONPs was increased, there was a corresponding increase in the active sites, thus accounting for the higher uptake of BRB from solution[62,73,74]. This in turn resulted in less saturation and less efficient use of the active sites of ZnONPs due to decreasing BRB
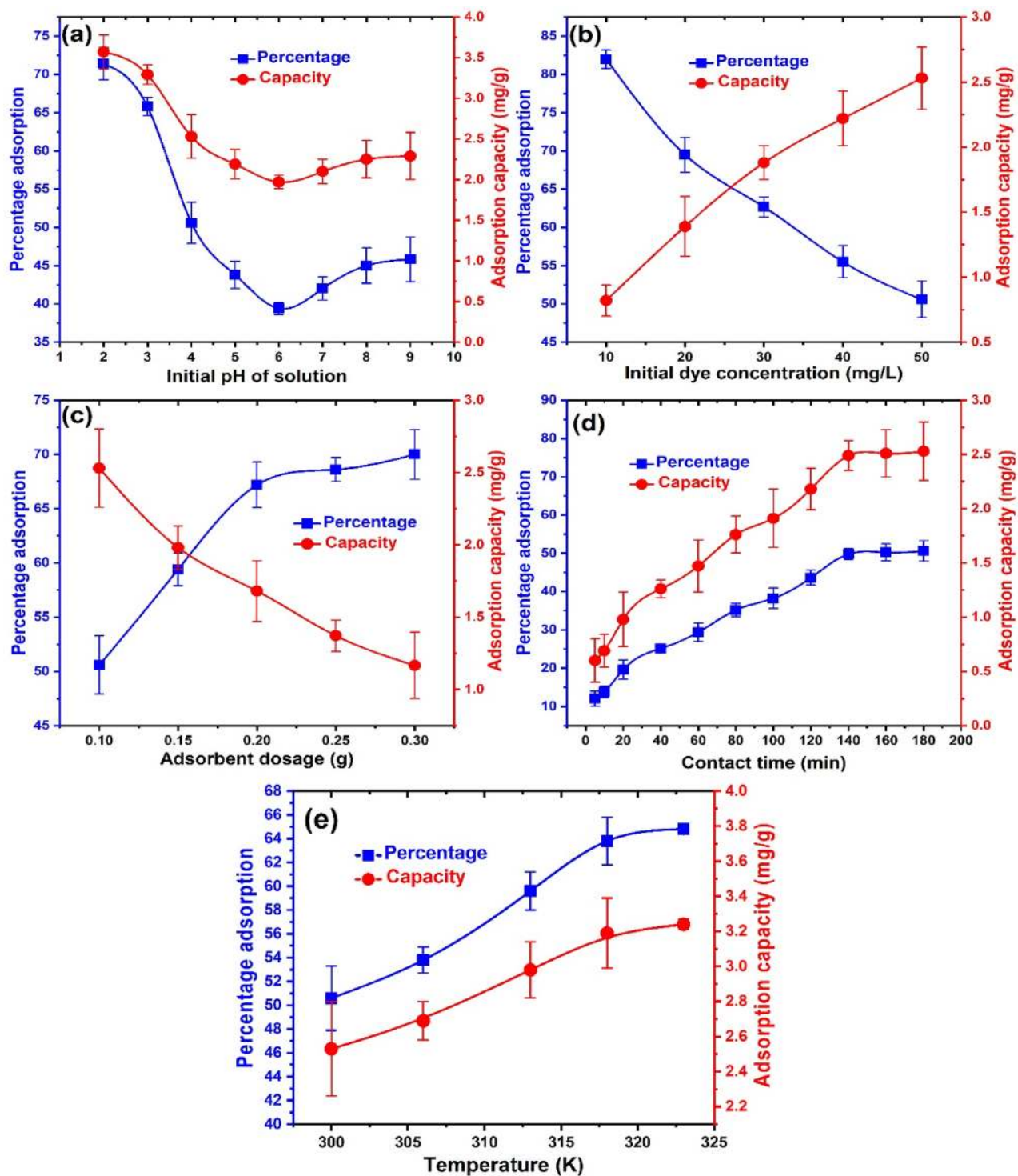
Figure 3. The influence of (**a**) solution pH (**b**) BRB concentration (**c**) ZnONPs dosage (**d**) contact time and (**e**) solution temperature on the removal of BRB onto ZnONPs.

concentration in solution[5,75]. Hence, we utilized ZnONPs dosage of 0.1 g to enable optimum use of the active sites of the adsorbent[68].

Figure 3d relates the influence of time on the removal of BRB onto ZnONPs. A steady increase in both the percentage adsorption and adsorption capacity with an increase in time from 5 to 140 min was obtained. Thereafter, there was no noticeable change in the uptake of BRB onto ZnONPs indicating that equilibrium was reached[76]. At the initial stages of adsorption, the ZnONPs sites were vacant and BRB concentration in solution was high[49]. This prompted a spontaneous interaction between the vacant sites and BRB molecules resulting in the initial rapid uptake. The interaction decreased with time due to the occupation of the sites of ZnONPs as well as the reducing dye concentration in solution. Eventually equilibrium was achieved, attributed to the saturation of the
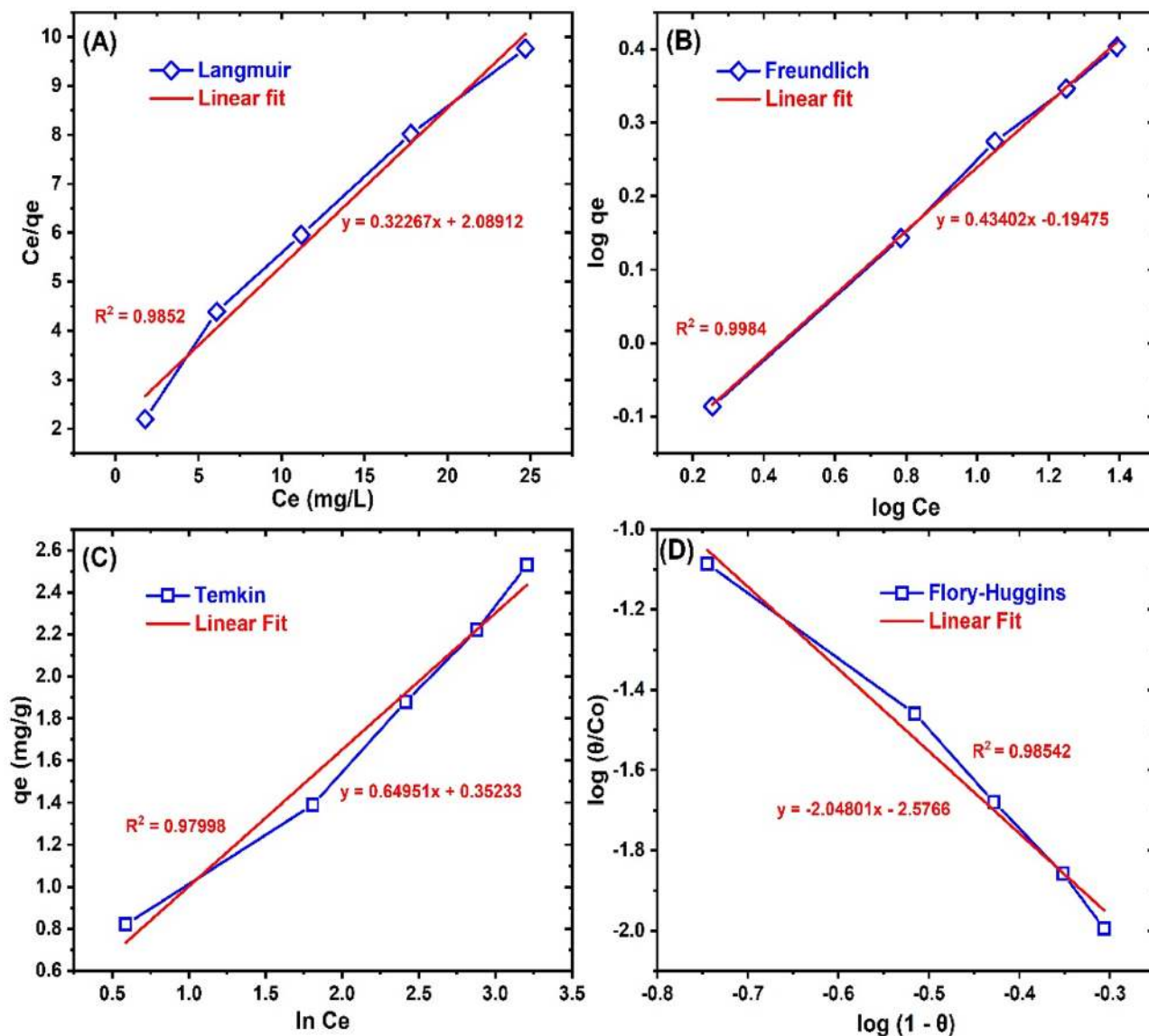
Figure 4. The (**A**) Langmuir (**B**) Freundlich (**C**) Temkin and (**D**) Flory–Huggins isotherm plots for the adsorption of BRP onto ZnONPs.

sites of ZnONPs[13]. A similar result was obtained in the abstraction of phenol from pharmaceutical and synthetic industrial wastewater onto ZnONPs[77]. We maintained an adsorption time of 180 min to enable equilibrium in the uptake of BRB from the solution. Furthermore, the influence of solution temperature on the removal of BRB onto the synthesized ZnONPs is illustrated in Fig. 3e. With an increase in solution temperature from 300 to 323 K, an increase in ZnONPs adsorption capacity from 50.6 to 64.8%, and percentage adsorption of BRB from 2.53 to 3.24 mg/g were achieved. This suggests that the uptake of BRB on ZnONPs is likely an endothermic one since it is favored at higher temperatures. The improved BRB uptake at higher temperatures could be attributed to enhanced interaction between the BRB species in solution and the adsorption sites of ZnONPs prompted by higher kinetic energy overcoming mass transfer resistances[78]. A similar finding was also documented in the uptake of As (III) from solution on ZnO nanorods[29].

Isotherm analysis of BRB adsorption. The adsorption isotherm modeling of BRB adsorption on the as-prepared ZnONPs was conducted to obtain useful information on the favorability of the adsorption process, nature of adsorption as well as potent interaction between the two phases[62,79]. This was analyzed by the Langmuir, Temkin, Freundlich, and Flory–Huggins models[80] as illustrated in Fig. 4. The calculated isotherm parameters obtained from the modeling are presented in Table 2. The best model fit was judged by the closer the R^2 value is to one and the smaller SSE values. The Langmuir model, which depicts a monolayer dye uptake on a homogenous material surface[49], presented a lower R^2 and higher SSE than the Freundlich model and thus was not applicable in the description of BRB adsorption onto ZnONPs. The Freundlich model gave the best fit to the process, presenting the highest R^2 of 0.9984 and lowest SSE of 0.0002. This implies a multilayer BRB uptake on

Model	Parameter	Value
Langmuir	K_L (L/g)	0.154
	q_L (g/g)	3.099
	R^2	0.9852
	SSE	0.5219
Freundlich	N	2.304
	K_F (L/kg)	0.639
	R^2	0.9984
	SSE	0.0002
Temkin	B(g/g)	0.6495
	A (L/kg)	1.720
	R^2	0.9799
	SSE	0.0368
Flory–Huggins	n_{FH}	− 2.048
	K_{FH}	0.0027
	R^2	0.9854
	SSE	0.0075

Table 2. The adsorption isotherm parameters for bromophenol blue adsorption onto ZnONPs.

a heterogeneous ZnONPs surface and that physisorption must have played a major role in the overall removal process[5]. This result was not consistent with the report of other researchers on the adsorption of heavy metals, phenol and, dyes onto ZnONPs[26,29,30,77,81–83]. They deduced that the Langmuir model was more appropriate indicating a monolayer uptake of the pollutants on ZnONPs. However, our result corroborated the report by Khosla et al.[84], that the Freundlich model presents a superior fit in the adsorption of anionic dyes (such as BRB) onto ZnONPs. Moreover, a good affinity between the adsorbent and pollutant in solution is usually indicated by the Freundlich *n* value within the range of 1–10[30]. From Table 2, the *n* value was 2.304, which indicated efficient interaction between BRB species in solution and the ZnONPs adsorbent. The favorability of the dye adsorption process was further tested by the application of the Langmuir separation factor $[R_L = (1/1 + K_LC_o)]$[74], where K_L is the Langmuir equilibrium adsorption constant[82]. The R_L value denotes a linear ($R_L = 1$), an irreversible ($R_L = 0$), a favorable ($0 < R_L < 1$) and unfavorable ($R_L > 1$) removal process[29]. The R_L value for BRB removal on ZnONPs was in the range of 0.115 to 0.394, which corroborates the favorable adsorption of BRB, indicating that ZnONPs are viable for the treatment of BRB polluted water. Besides, the monolayer uptake capacity of ZnONPs for BRB was 3.099 mg/g, which is higher than that of activated charcoal (0.081 mg/g)[85] and polymeric gel (2.99 mg/g)[86] but lower than 22.72 mg/g obtained for chitin nanoparticle[87]. Thus, the simple preparation procedure as well as potent antifungal properties (see discussion in the "Antifungal activity" section) would be the advantage in the application of ZnONPs for BRB wastewater treatment.

Kinetics and thermodynamics of adsorption. The kinetic modeling of adsorption processes helps in the calculation of kinetic parameters, which is useful in system design and provides useful information on sorption mechanism[88]. The kinetics of BRB adsorption onto ZnONPs was modeled by the PFO, PSO, LFD, and IPD equations. The kinetic plots are presented in Fig. 5 while the obtained kinetic parameters are given in Table 3. It is obvious from the R^2 of 0.9495 and the SSE of 0.7411 that the PSO was more suited than the PFO model in the kinetic description of BRB uptake onto ZnONPs. This was also supported by the closer calculated qe (3.0597 mg/g) of the PSO to the experimental qe (2.53 mg/g), than that presented by the PFO model (3.4883 mg/g). The best fit presented by the PSO models suggests the involvement of electrostatic interactions between the BRB molecules in solution and ZnONPs in the dye removal process[89,90]. This implication corroborates our deduction from the FTIR analysis obtained after BRB adsorption onto ZnONPs, which showed the involvement of electrostatic interactions. A similar result was reported in the adsorption of methylene blue onto ZnONPs impregnated sawdust based cellulose nanocrystals[91].

Furthermore, the LFD and IPD models provide reliable information about the diffusion mechanism of adsorption[62]. Comparing the two diffusion models, it is evident that the IPD model was best fitted to the diffusion process of BRB molecules onto ZnONPs as inferred from the high R^2 (0.9889) and low SSE (0.0581). This indicates that the diffusion of BRB through the surface pores of ZnONPs played a more vital role in the overall adsorption process than the boundary layer diffusion. However, the occurrence of the intercept (0.1215), showed that particle diffusion was not solely responsible for BRB uptake, but to some extent involves film diffusion[30,49]. A similar finding in the adsorption of BRB onto *Solanum tuberosum* peel—silver nanoparticle hybrid was reported in our previous work[8]. The ultra-sonication applied prompted potent interaction between the dye species and the particle pores thus enhancing the particle diffusion mechanism. In addition, this observation is in line with the pore and SEM analysis, which showed a porous nature of ZnONPs that, would enhance the dye uptake from the solution.

The thermodynamics of BRB adsorption on ZnONPs was also evaluated from the Van't Hoff plot as illustrated in Fig. 5E. The calculated thermodynamic parameters such as the changes in enthalpy (ΔH°), entropy (ΔS°),
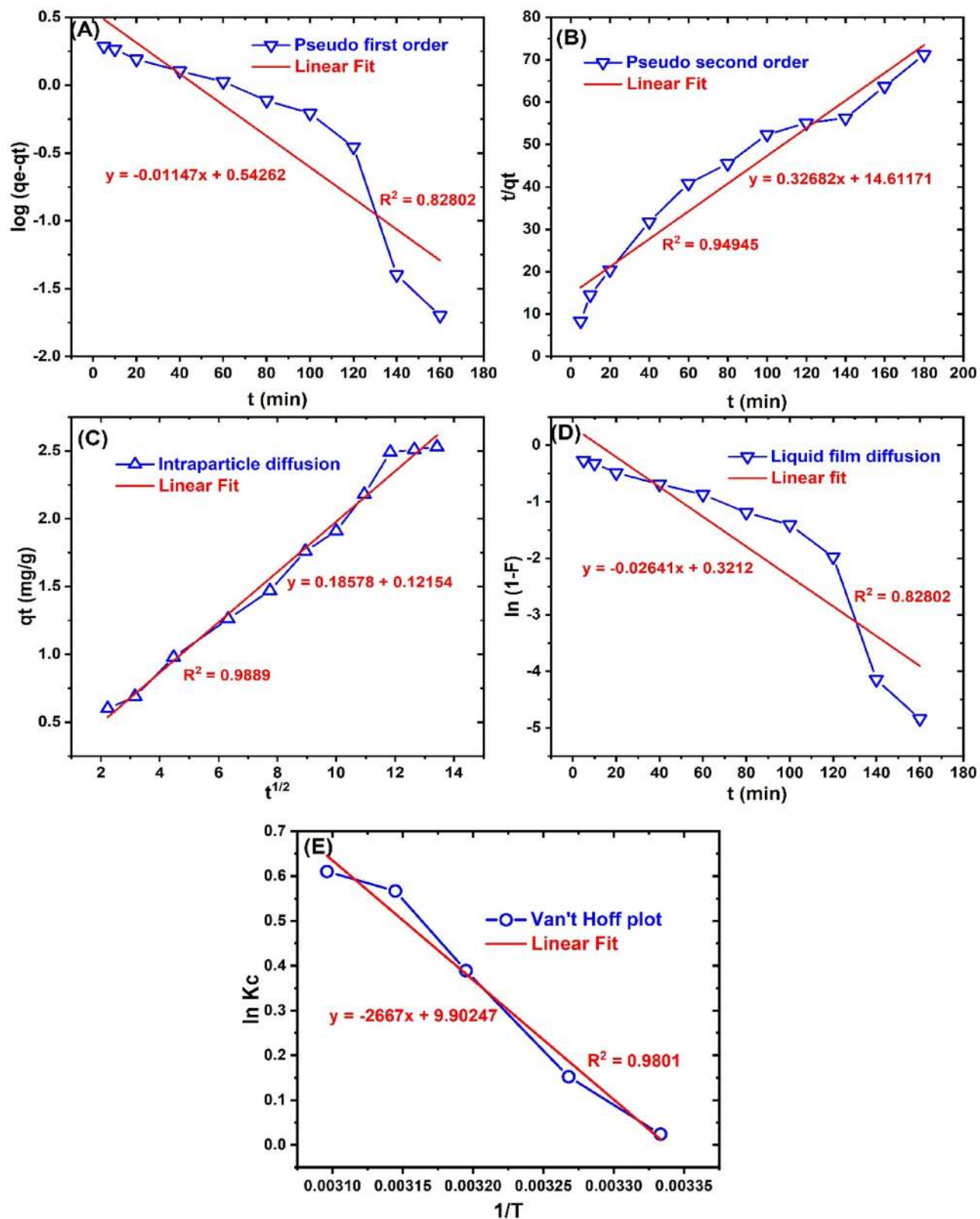
Figure 5. The (**A**) Pseudo-first-order, (**B**) Pseudo-second order, (**C**) Intraparticle diffusion, (**D**) liquid film diffusion and (**E**) Van't Hoff plots for the adsorption of BRP onto ZnONPs.

and free energy (ΔG^o) were used to analyze the spontaneity, randomness, and the physical or chemical nature of BRB uptake onto the synthesized ZnONPs[92]. The thermodynamic parameters obtained are presented in Table 4.

Model	Parameter	Value
Pseudo-first order	$qe_{(exp)}$ (mg/g)	2.53
	K_I (min⁻¹)	0.0264
	$qe_{(cal)}$ (mg/g)	3.4883
	R^2	0.8280
	SSE	0.7569
Pseudo-second-order	K_2 (g/mg min)	0.0073
	qe_{cal} (mg/g)	3.0597
	R^2	0.9495
	SSE	0.7411
Intraparticle diffusion	K_d (mg/g min⁻¹ᐟ²)	0.1858
	C	0.1215
	R^2	0.9889
	SSE	0.0581
Liquid film diffusion	K_{fd}	0.0264
	Y	0.3212
	R^2	0.8280
	SSE	4.0134

Table 3. The kinetic parameters for bromophenol blue adsorption onto ZnONPs.

Temp (K)	K_c	ΔG^o (kJ/mol)	ΔH^o (kJ/mol)	ΔS^o (J/(mol K))	R^2
300	1.024	− 0.059	22.173	74.02	0.9801
306	1.165	− 0.387			
313	1.475	− 1.012			
318	1.762	− 1.498			
323	1.841	− 1.638			

Table 4. Thermodynamic parameters for bromophenol blue adsorption onto ZnONPs.

It is evident that the adsorption of BRB on the prepared ZnONPs adsorbent is spontaneous as the ΔG^o values were negative at all temperatures[93]. Again, the increase in negativity of the ΔG^o values with temperature increase shows that high temperature is favorable for BRB uptake[94]. Also, the positive ΔH^o value recorded is a clear indication of the endothermic nature of the dye adsorption on ZnONPs[95], which corroborates increasing BRB uptake with temperature increase (Fig. 3e). This result is consistent with other studies depicting the endothermic adsorption of As(III)[29], azo dyes[30] and, Pb(II) ions[83] on ZnONPs. It is important to mention that ΔH^o values in the range of 2.1–20.9 kJ/mol and 80–200 kJ/mol are attributed to physisorption and chemisorption respectively[96]. The ΔH^o of 22.173 kJ/mol obtained for the removal was slightly higher than the physisorption range but far lower than the chemisorption range. This indicated physicochemical adsorption of BRB onto ZnONPs rather than a purely chemical or physical uptake, dominated mainly by the physical forces of adsorption[97]. Again, this implies that a much lower energy barrier is to be overcome in the desorption of the BRB loaded ZnONPs during the regeneration of the adsorbent, compared to adsorption processes dominated or controlled by chemisorption. Furthermore, the increasing randomness at the ZnONPs-BRB solution interface was indicated by the positive ΔS^o value of 74.02 J/(mol K)[98]. This increasing random interaction at the interface must have enhanced efficient interaction between BRB molecules and the particle pores of ZnONPs, which accounted for the dominant role played by intraparticle diffusion in the overall adsorption process. Such increasing randomness is well documented in the adsorption of dyes onto ZnONPs based adsorbents[47,99–101].

Antifungal activity. The antifungal activity of the ZnONPs was tested for possible application as simultaneous BRB removal and antifungal treatment of wastewater. Noticeably, as shown in Fig. 6, all of the tested concentrations of ZnONPs showed inhibitory effects on the three cultures, and the zones of inhibition increased consistently as the concentration of ZnONPs increased (Table 5). The strain *A. alternata* CGJM 3076 showed maximum susceptibility towards ZnONPs (0.002–5 mg/mL), as depicted by the largest zone of inhibition range from 25.09 to 36.28 mm. This was followed by *F. verticilliodes* CGJM 3823 (range from 23.77 to 34.77 mm) and *A. alternata* CGJM3078 (range from 22.73 to 30.63 mm). Concurrently, all the positive controls [bleach (5%)] exhibited similar diameter in their zones of inhibitions than those of ZnONPs, while none of the negative control (sterile water) showed effects**.**

Significantly less volumes of ZnONPs (40 μL) were used against all the tested fungi in this study in comparison to a previous study[33], where 100 μL volume was implemented for an identical concentrations range (0.002–5 mg/mL). The enhanced antifungal efficiency of the formulated ZnONPs in the current study is possibly based on
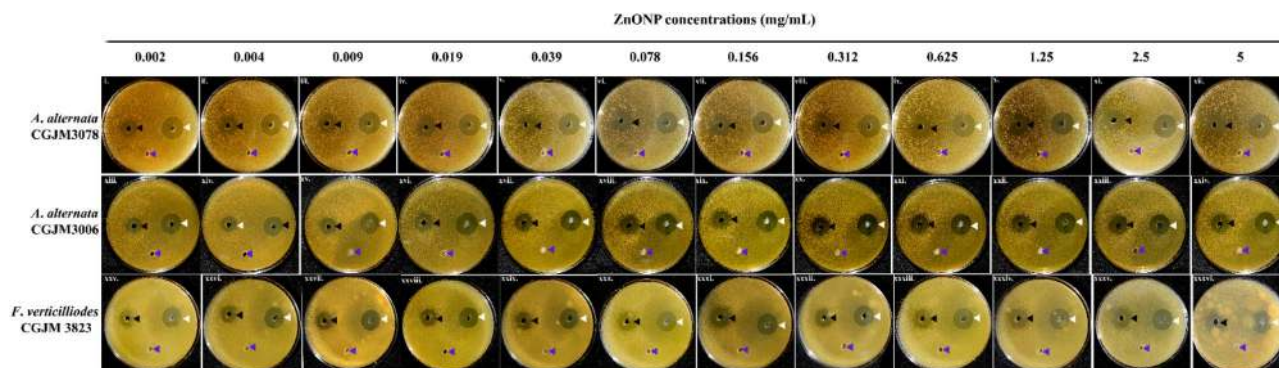
Figure 6. Plates representing the inhibition zones across a concentration range of ZnONPs against the fungal strains *Alternaria alternata* CGJM3078 (i–xii), *A. alternata* CGJM3006 (xiii–xxiv) and *Fusarium verticilliodes* CGJM 3823 (xxv–xxxvi). Black arrow heads indicate antimicrobial activities caused by ZnONPs, white indicates the bleach positive control, and blue indicates the sterile distilled water.

| ZnONPs (mg/mL) | Zone of Inhibition (mm) | | | | | |
	Alternaria alternata CGJM3078	Bleach (5%) (positive control)	*Alternaria alternata* CGJM3006	Bleach (5%) (positive control)	*Fusarium verticilliodes* CGJM 3823	Bleach (5%) (positive control)
0.002	22.73	37.68	25.09	39.80	23.77	36.58
0.004	23.91	38.56	28.13	38.91	25.57	35.82
0.009	25.06	35.88	29.09	37.64	25.58	36.15
0.019	25.98	39.18	29.17	37.81	26.98	36.12
0.039	27.23	36.47	29.49	38.39	26.99	37.08
0.078	28.55	35.32	31.23	38.51	27.73	35.94
0.156	28.92	34.91	32.17	39.56	28.45	35.60
0.312	29.19	35.98	32.19	37.33	29.00	35.38
0.625	29.82	34.29	33.04	39.66	29.09	35.83
1.25	29.98	33.67	33.08	38.32	31.06	35.28
2.5	30.32	33.42	34.36	37.71	31.80	38.44
5	30.63	37.26	36.28	40.93	34.77	37.00

Table 5. Antifungal activities (in vitro) of ZnONPs against the filamentous fungi *Alternaria alternata* (CGJM3078 andCGJM3006) and *Fusarium verticilliodes* CGJM 3823 are indicated in the form of inhibition zone sizes for each concentration of ZnONPs treatment. Bleach served as the positive control that exhibited similar diameter in their zones of inhibitions. The negative controls all did not show any activity.

factors such as the size and shape of the particles, a large surface area to volume ratio that improved the solubility of the nanoparticles in comparison to the larger ones, the generation of reactive oxygen species (ROS) and the effective release of Zn^{2+} ions[51].

The exact underlying molecular mechanisms of ZnONPs antifungal activities are yet to be elucidated[102]. In this study we proposed a few plausible mechanisms (Fig. 7). Zn^{2+} can possibly be released from the surface of ZnONPs, as it has been shown in AgNPs[103] that interacted with the fungal cell wall, passed and accumulated in the cytoplasm. This causes cell metabolism disturbances, impairment of the nucleic acid material by their irreversible adherence, ribosome disassembly, protein denaturations, electron chain disruptions, all of which ultimately resulting in cell death (Fig. 7). The interactions may also cause deformed fungal hyphae with ruptures and unusual bulging as was observed in an SEM study of antifungal activities of Zn compounds against pathogenic fungal strains of *Fusarium graminearum*, *Penicillium citrinum* and *Aspergillus flavus*[104]. The generation of the reactive oxygen species (ROS) (Fig. 7) as per a previous study[51], can cause lipid peroxidation, leading to cell death. Simultaneously, the fungal cell wall can become more permeable because of the Zn^{2+}, resulting in subsequent leakage of the plasma fluid and cellular organelles causing cellular senescence (Fig. 7). SEM structure imaging of the ZnONPs developed in the present study revealed the average size of ZnONPs as 65.3 nm. This is consistent with the previous findings[31], where the average size was reported as 70 ± 15 nm. Those ZnONPs successfully inhibited the growth of mycotoxin producing fungi, *Botrytis cinerea* and *Penicillium expansum*, causing cellular perturbations, and fungal hyphal distortion.
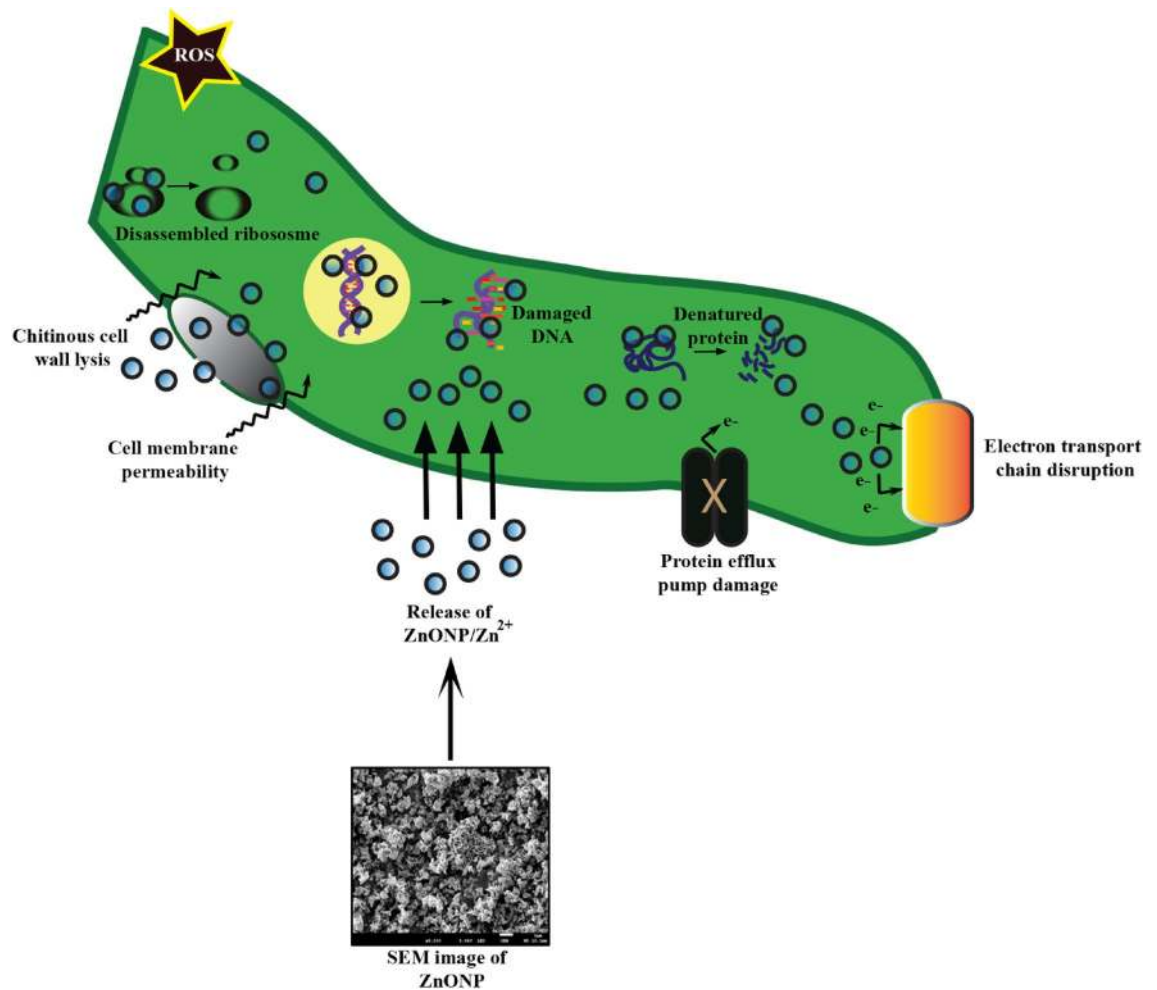
Figure 7. Schematic representation of the possible mechanism causing the antifungal ability of ZnONPs on a single fungal cell.

Conclusions

Zinc oxide nanoparticles (ZnONPs) were synthesized in a- simple one-pot system and applied for the adsorption of bromophenol blue (BRB) and as an antifungal agent against *Alternaria alternata* and *Fusarium verticilliodes* filamentous fungi. The FTIR showed the presence of the O–H and Zn–O bands on the synthesized ZnONPs, which were responsible for the adsorption of BRB via electrostatic, hydrophobic, and weak Vander Waals interaction. The XRD, UV, and EDX characterizations showed the successful synthesis of the ZnONPs. Thermal analysis revealed high thermal stability of the ZnONPs with a 22.92% weight loss at 800 °C, while BET analysis showed sufficient surface area and pore properties desirable for efficient BRB uptake from solution. The SEM and TEM morphology displayed an irregular shaped and aggregated porous structure of ZnONPs. The solution temperature, pH, time, BRB concentration, and ZnONPs dosage were found to influence significantly the BRB uptake on ZnONPs. The operating conditions were selected as pH, temperature, time, dosage, and concentration of 4.0, 300 K, 180 min, 0.1 g, and 50 mg/L respectively. The Freundlich model presented the best fit to the isotherm analysis for the adsorption process compared to the Langmuir, Flory Huggins, and Temkin isotherm models. For kinetic analysis of BRB adsorption onto ZnONPs, the pseudo-second-order and intra-particle-diffusion were better fitted than the Pseudo-first-order and liquid-film-diffusion models. A feasible, spontaneous, random, and endothermic removal of BRB onto ZnONPs was revealed from the thermodynamic evaluation of the process. The synthesized ZnONPs were found to be efficient in the adsorption of BRB from solution with a maximum monolayer uptake capacity of 3.099 mg/g, which was higher than some previously reported adsorbents.

In addition, the prepared ZnONPs exhibited potent antifungal activities against the filamentous fungi, *A. alternata* and *F. verticilliodes*. The antifungal effects, such as inhibition of growth and reproduction of the filamentous fungi, are enhanced significantly with the ZnO nanostructures. Therefore, the present study, together with previous studies, showed that ZnONPs have tremendous potential as an effective postharvest disease control antifungal agents against filamentous fungi, or even possibly in the field. No studies have, however, tested this in vivo.

References

1. Tohamy, H.-A.S., El-Sakhawy, M. & Kamel, S. Carboxymethyl cellulose-grafted graphene oxide/polyethylene glycol for efficient Ni(II) adsorption. *J. Polym. Environ.* https://doi.org/10.1007/s10924-020-01920-7 (2020).
2. Al-Ghouti, M. A. & Al-Absi, R. S. Mechanistic understanding of the adsorption and thermodynamic aspects of cationic methylene blue dye onto cellulosic olive stones biomass from wastewater. *Sci. Rep.* **10**, 15928 (2020).
3. Tian, B., Hua, S., Tian, Y. & Liu, J. Cyclodextrin-based adsorbents for the removal of pollutants from wastewater: A review. *Environ. Sci. Pollut. Res.* https://doi.org/10.1007/s11356-020-11168-2 (2020).
4. Dotto, G. L. & McKay, G. Current scenario and challenges in adsorption for water treatment. *J. Environ. Chem. Eng.* **8**, 103988 (2020).
5. Akpomie, K. G. & Conradie, J. Banana peel as a biosorbent for the decontamination of water pollutants. A review. *Environ. Chem. Lett.* **18**, 1085–1112 (2020).
6. Yagub, M. T., Sen, T. K., Afroze, S. & Ang, H. M. Dye and its removal from aqueous solution by adsorption: A review. *Adv. Colloid Interface Sci.* **209**, 172–184 (2014).
7. Mirzaei, D., Zabardasti, A., Mansourpanah, Y., Sadeghi, M. & Farhadi, S. Efficacy of novel NaX/MgO–TiO2 zeolite nanocomposite for the adsorption of methyl orange (MO) dye: Isotherm, kinetic and thermodynamic studies. *J. Inorg. Organomet. Polym. Mater.* **30**, 2067–2080 (2020).
8. Akpomie, K. G. & Conradie, J. Biogenic and chemically synthesized *Solanum tuberosum* peel–silver nanoparticle hybrid for the ultrasonic aided adsorption of bromophenol blue dye. *Sci. Rep.* **10**, 17094 (2020).
9. Wang, J. *et al.* Preparation and excellent adsorption of water pollution dyes over magnetic Fe₃O₄/C nanoparticles with hollow grape cluster morphology. *J. Nanoparticle Res.* **22**, 196 (2020).
10. Mok, C. F. *et al.* Adsorption of dyes using poly(vinyl alcohol) (PVA) and PVA-based polymer composite adsorbents: A review. *J. Polym. Environ.* **28**, 775–793 (2020).
11. El-Gamal, S. M. A., Amin, M. S. & Ahmed, M. A. Removal of methyl orange and bromophenol blue dyes from aqueous solution using Sorel's cement nanoparticles. *J. Environ. Chem. Eng.* **3**, 1702–1712 (2015).
12. Akpomie, K. G. & Conradie, J. Efficient synthesis of magnetic nanoparticle-*Musa acuminata* peel composite for the adsorption of anionic dye. *Arab. J. Chem.* **13**, 7115–7131 (2020).
13. Saghian, M., Dehghanpour, S. & Sharbatdaran, M. Unique and efficient adsorbents for highly selective and reverse adsorption and separation of dyes via the introduction of SO₃H functional groups into a metal–organic framework. *RSC Adv.* **10**, 9369–9377 (2020).
14. Song, Y.-B., Song, X.-D., Cheng, C.-J. & Zhao, Z.-G. Poly(4-styrenesulfonic acid-co-maleic acid)-sodium-modified magnetic reduced graphene oxide for enhanced adsorption performance toward cationic dyes. *RSC Adv.* **5**, 87030–87042 (2015).
15. Ani, J. U. *et al.* Potentials of activated carbon produced from biomass materials for sequestration of dyes, heavy metals, and crude oil components from aqueous environment. *Appl. Water Sci.* **10**, 1–11 (2020).
16. Song, F. *et al.* Adsorption kinetics and thermodynamics of Ni(II) by Pisha sandstone. *J. Nanoparticle Res.* **22**, 179 (2020).
17. Anastopoulos, I., Hosseini-Bandegharaei, A., Fu, J., Mitropoulos, A. C. & Kyzas, G. Z. Use of nanoparticles for dye adsorption: Review. *J. Dispers. Sci. Technol.* **39**, 836–847 (2018).
18. Kausar, A. *et al.* Dyes adsorption using clay and modified clay: A review. *J. Mol. Liq.* **256**, 395–407 (2018).
19. Reyes-Ledezma, J. L., Uribe-Ramírez, D., Cristiani-Urbina, E. & Morales-Barrera, L. Biosorptive removal of acid orange 74 dye by HCl-pretreated *Lemna* sp. *PLoS ONE* **15**, e0228595 (2020).
20. Wong, S. *et al.* Effective removal of anionic textile dyes using adsorbent synthesized from coffee waste. *Sci. Rep.* **10**, 2928 (2020).
21. David, M. K., Okoro, U. C., Akpomie, K. G., Okey, C. & Oluwasola, H. O. Thermal and hydrothermal alkaline modification of kaolin for the adsorptive removal of lead(II) ions from aqueous solution. *SN Appl. Sci.* **2**, 1134 (2020).
22. Cui, Z., Zhang, J., Xue, Y. & Duan, H. Size-dependent thermodynamics and kinetics of adsorption on nanoparticles: A theoretical and experimental study. *Langmuir* **34**, 3197–3206 (2018).
23. Marimuthu, S. *et al.* Silver nanoparticles in dye effluent treatment: A review on synthesis, treatment methods, mechanisms, photocatalytic degradation, toxic effects and mitigation of toxicity. *J. Photochem. Photobiol. B Biol.* **205**, 111823 (2020).
24. Al-Aoh, H. A. Adsorption performances of nickel oxide nanoparticles (NiO NPs) towards bromophenol blue dye (BB). *Desalin. Water Treat.* **110**, 229–238 (2018).
25. Ahmed, M. A. & Abou-Gamra, Z. M. Mesoporous MgO nanoparticles as a potential sorbent for removal of fast orange and bromophenol blue dyes. *Nanotechnol. Environ. Eng.* **1**, 10 (2016).
26. Gu, M. *et al.* The selective heavy metal ions adsorption of zinc oxide nanoparticles from dental wastewater. *Chem. Phys.* **534**, 110750 (2020).
27. Akbar, A. *et al.* Synthesis and antimicrobial activity of zinc oxide nanoparticles against foodborne pathogens Salmonella typhimurium and Staphylococcus aureus. *Biocatal. Agric. Biotechnol.* **17**, 36–42 (2019).
28. Alkasir, M. *et al.* Evaluation cytotoxicity effects of biosynthesized zinc oxide nanoparticles using aqueous Linum Usitatissimum extract and investigation of their photocatalytic activityackn. *Inorg. Chem. Commun.* **119**, 108066 (2020).
29. Yuvaraja, G., Prasad, C., Vijaya, Y. & Subbaiah, M. V. Application of ZnO nanorods as an adsorbent material for the removal of As(III) from aqueous solution: Kinetics, isotherms and thermodynamic studies. *Int. J. Ind. Chem.* **9**, 17–25 (2018).
30. Zafar, M. N. *et al.* Effective adsorptive removal of azo dyes over spherical ZnO nanoparticles. *J. Mater. Res. Technol.* **8**, 713–725 (2019).
31. He, L., Liu, Y., Mustapha, A. & Lin, M. Antifungal activity of zinc oxide nanoparticles against *Botrytis cinerea* and *Penicillium expansum*. *Microbiol. Res.* **166**, 207–215 (2011).
32. Arciniegas-Grijalba, P. A., Patiño-Portela, M. C., Mosquera-Sánchez, L. P., Guerrero-Vargas, J. A. & Rodríguez-Páez, J. E. ZnO nanoparticles (ZnO-NPs) and their antifungal activity against coffee fungus Erythricium salmonicolor. *Appl. Nanosci.* **7**, 225–241 (2017).
33. De la Rosa-García, S. C. *et al.* Antifungal activity of ZnO and MgO nanomaterials and their mixtures against *Colletotrichum gloeosporioides* strains from tropical fruit. *J. Nanomater.* **2018**, 1–9 (2018).
34. de Souza, R. C., Haberbeck, L. U., Riella, H. G., Ribeiro, D. H. B. & Carciofi, B. A. M. Antibacterial activity of zinc oxide nanoparticles synthesized by solochemical process. *Braz. J. Chem. Eng.* **36**, 885–893 (2019).
35. Khatami, M. *et al.* Applications of green synthesized Ag, ZnO and Ag/ZnO nanoparticles for making clinical antimicrobial wound-healing bandages. *Sustain. Chem. Pharm.* **10**, 9–15 (2018).
36. Gambino, M., Ahmed, M. A. A., Villa, F. & Cappitelli, F. Zinc oxide nanoparticles hinder fungal biofilm development in an ancient Egyptian tomb. *Int. Biodeterior. Biodegradation* **122**, 92–99 (2017).
37. Sardella, D., Gatt, R. & Valdramidis, V. P. Physiological effects and mode of action of ZnO nanoparticles against postharvest fungal contaminants. *Food Res. Int.* **101**, 274–279 (2017).
38. Reddy, M. V. B., Angers, P., Castaigne, F. & Arul, J. Chitosan effects on blackmold rot and pathogenic factors produced by *Alternaria alternata* in postharvest tomatoes. *J. Am. Soc. Hortic. Sci.* **125**, 742–747 (2000).

39. Tsuge, T. *et al.* Host-selective toxins produced by the plant pathogenic fungus *Alternaria alternata*. *FEMS Microbiol. Rev.* **37**, 44–66 (2013).

40. Pastor, F. J. & Guarro, J. Alternaria infections: Laboratory diagnosis and relevant clinical features. *Clin. Microbiol. Infect.* **14**, 734–746 (2008).

41. Baldwin, T. T. *et al.* Maize seedling blight induced by fusarium verticillioides: Accumulation of fumonisin B 1 in leaves without colonization of the leaves. *J. Agric. Food Chem.* **62**, 2118–2125 (2014).

42. van Rensburg, B. J., McLaren, N. W., Schoeman, A. & Flett, B. C. The effects of cultivar and prophylactic fungicide spray for leaf diseases on colonisation of maize ears by fumonisin producing *Fusarium* spp. and fumonisin synthesis in South Africa. *Crop Prot.* **79**, 56–63 (2016).

43. Zhang, L., Wang, J., Zhang, C. & Wang, Q. Analysis of potential fumonisin-producing *Fusarium* species in corn products from three main maize-producing areas in eastern China. *J. Sci. Food Agric.* **93**, 693–701 (2013).

44. Gallo, A., Giuberti, G., Frisvad, J., Bertuzzi, T. & Nielsen, K. Review on mycotoxin issues in ruminants: Occurrence in Forages, Effects of mycotoxin ingestion on health status and animal performance and practical strategies to counteract their negative effects. *Toxins* **7**, 3057–3111 (2015).

45. Marin, S., Ramos, A. J., Cano-Sancho, G. & Sanchis, V. Mycotoxins: Occurrence, toxicology, and exposure assessment. *Food Chem. Toxicol.* **60**, 218–237 (2013).

46. Wu, F. Measuring the economic impacts of *Fusarium* toxins in animal feeds. *Anim. Feed Sci. Technol.* **137**, 363–374 (2007).

47. Akpomie, K. G. & Conradie, J. Synthesis, characterization, and regeneration of an inorganic–organic nanocomposite (ZnO@biomass) and its application in the capture of cationic dye. *Sci. Rep.* **10**, 14441 (2020).

48. Jiao, Y. *et al.* Characterization of pine-sawdust pyrolytic char activated by phosphoric acid through microwave irradiation and adsorption property toward CDNB in batch mode. *Desalin. Water Treat.* **77**, 247–255 (2017).

49. Ezekoye, O. M. *et al.* Biosorptive interaction of alkaline modified Dialium guineense seed powders with ciprofloxacin in contaminated solution: Central composite, kinetics, isotherm, thermodynamics, and desorption. *Int. J. Phytoremediation* **22**, 1028–1037 (2020).

50. Ghosh, S. *et al.* In situ cultured bacterial diversity from iron curtain cave, Chilliwack, British Columbia, Canada. *Diversity* **9**, 36 (2017).

51. Kumar, P. *et al.* Optical and surface properties of Zn doped CdO nanorods and antimicrobial applications. *Colloids Surf. A Physicochem. Eng. Asp.* **605**, 125369 (2020).

52. Khatami, M., Alijani, H. Q., Heli, H. & Sharifi, I. Rectangular shaped zinc oxide nanoparticles: Green synthesis by Stevia and its biomedical efficiency. *Ceram. Int.* **44**, 15596–15602 (2018).

53. Miri, A., Mahdinejad, N., Ebrahimy, O., Khatami, M. & Sarani, M. Zinc oxide nanoparticles: Biosynthesis, characterization, antifungal and cytotoxic activity. *Mater. Sci. Eng. C* **104**, 109981 (2019).

54. Selim, Y. A., Azb, M. A., Ragab, I. & Abd El-Azim, H. M. Green synthesis of zinc oxide nanoparticles using aqueous extract of *Deverra tortuosa* and their cytotoxic activities. *Sci. Rep.* **10**, 3445 (2020).

55. Jayappa, M. D. *et al.* Green synthesis of zinc oxide nanoparticles from the leaf, stem and in vitro grown callus of *Mussaenda frondosa* L.: characterization and their applications. *Appl. Nanosci.* **10**, 3057–3074 (2020).

56. Sharifalhoseini, Z., Entezari, M. H. & Jalal, R. Direct and indirect sonication affect differently the microstructure and the morphology of ZnO nanoparticles: Optical behavior and its antibacterial activity. *Ultrason. Sonochem.* **27**, 466–473 (2015).

57. Ramimoghadam, D., Hussein, M. Z. & Taufiq-Yap, Y. H. Synthesis and characterization of ZnO nanostructures using palm olein as biotemplate. *Chem. Cent. J.* **7**, 71 (2013).

58. Zare, E., Pourseyedi, S., Khatami, M. & Darezereshki, E. Simple biosynthesis of zinc oxide nanoparticles using nature's source, and it's in vitro bio-activity. *J. Mol. Struct.* **1146**, 96–103 (2017).

59. Khatami, M. *et al.* Greener synthesis of rod shaped zinc oxide NPs using Lilium ledebourii tuber and evaluation of their leishmanicidal activity. *Iran. J. Biotechnol.* **18**, 1–5 (2020).

60. Ali, I., Peng, C. & Naz, I. Removal of lead and cadmium ions by single and binary systems using phytogenic magnetic nanoparticles functionalized by 3-marcaptopropanic acid. *Chinese J. Chem. Eng.* **27**, 949–964 (2019).

61. Malakootian, M., Khatami, M., Mahdizadeh, H., Nasiri, A. & Amiri Gharaghani, M. A study on the photocatalytic degradation of p-Nitroaniline on glass plates by Thermo-Immobilized ZnO nanoparticle. *Inorg. Nano Metal Chem.* **50**, 124–135 (2020).

62. Chukwuemeka-Okorie, H. O., Ekemezie, P. N., Akpomie, K. G. & Olikagu, C. S. Calcined corncob-kaolinite Combo as new sorbent for sequestration of toxic metal ions from polluted aqua media and desorption. *Front. Chem.* **6**, 1–13 (2018).

63. Haque, M. J., Bellah, M. M., Hassan, M. R. & Rahman, S. Synthesis of ZnO nanoparticles by two different methods & comparison of their structural, antibacterial, photocatalytic and optical properties. *Nano Express* **1**, 010007 (2020).

64. Mahamuni, P. P. *et al.* Synthesis and characterization of zinc oxide nanoparticles by using polyol chemistry for their antimicrobial and antibiofilm activity. *Biochem. Biophys. Rep.* **17**, 71–80 (2019).

65. Afroze, S. & Sen, T. K. A review on heavy metal ions and dye adsorption from water by agricultural solid waste adsorbents. *Water. Air. Soil Pollut.* **229**, 7 (2018).

66. Joudi, M. *et al.* Synthesis of an efficient hydroxyapatite–chitosan–montmorillonite thin film for the adsorption of anionic and cationic dyes: Adsorption isotherm, kinetic and thermodynamic study. *SN Appl. Sci.* **2**, 1078 (2020).

67. Akpomie, K. G., Dawodu, F. A. & Adebowale, K. O. Mechanism on the sorption of heavy metals from binary-solution by a low cost montmorillonite and its desorption potential. *Alexandria Eng. J.* **54**, 757–767 (2015).

68. Akpomie, K. G. & Dawodu, F. A. Physicochemical analysis of automobile effluent before and after treatment with an alkaline-activated montmorillonite. *J. Taibah Univ. Sci.* **9**, 465–476 (2015).

69. Silva, F. *et al.* Biosorption of methylene blue dye using natural biosorbents made from weeds. *Materials* **12**, 2486 (2019).

70. Cai, C.-X. *et al.* A novel approach of utilization of the fungal conidia biomass to remove heavy metals from the aqueous solution through immobilization. *Sci. Rep.* **6**, 36546 (2016).

71. Chukwuemeka-Okorie, H. O., Ekuma, F. K., Akpomie, K. G., Nnaji, J. C. & Okereafor, A. G. Adsorption of tartrazine and sunset yellow anionic dyes onto activated carbon derived from cassava sievate biomass. *Appl. Water Sci.* **11**, 27 (2021).

72. Lin, D. *et al.* Adsorption of dye by waste black tea powder: Parameters, kinetic, equilibrium, and thermodynamic studies. *J. Chem.* **2020**, 1–13 (2020).

73. Rokni, S., Haji Seyed Mohammad Shirazi, R., Miralinaghi, M. & Moniri, E. Efficient adsorption of anionic dyes onto magnetic graphene oxide coated with polyethylenimine: Kinetic, isotherm, and thermodynamic studies. *Res. Chem. Intermed.* **46**, 2247–2274 (2020).

74. Raghav, S. & Kumar, D. Adsorption equilibrium, kinetics, and thermodynamic studies of fluoride adsorbed by tetrametallic oxide adsorbent. *J. Chem. Eng. Data* **63**, 1682–1697 (2018).

75. Hamzezadeh, A., Rashtbari, Y., Afshin, S., Morovati, M. & Vosoughi, M. Application of low-cost material for adsorption of dye from aqueous solution. *Int. J. Environ. Anal. Chem.* https://doi.org/10.1080/03067319.2020.1720011 (2020).

76. Dawodu, F. A., Abonyi, C. J. & Akpomie, K. G. Feldspar-banana peel composite adsorbent for efficient crude oil removal from solution. *Appl. Water Sci.* **11**, 3 (2021).

77. Sridar, R., Ramanane, U. U. & Rajasimman, M. ZnO nanoparticles: Synthesis, characterization and its application for phenol removal from synthetic and pharmaceutical industry wastewater. *Environ. Nanotechnol. Monit. Manag.* **10**, 388–393 (2018).

78. Mustapha, S. *et al.* Adsorption isotherm, kinetic and thermodynamic studies for the removal of Pb(II), Cd(II), Zn(II) and Cu(II) ions from aqueous solutions using Albizia lebbeck pods. *Appl. Water Sci.* **9**, 142 (2019).

79. Akpomie, K. G. *et al.* Equilibrium isotherms modeling of crude oil sorption from aqua mixture onto *Codiaeum variegatum* stem powder. *Pet. Sci. Technol.* **37**, 329–336 (2019).

80. Eze, S. I. *et al.* Antibiotic adsorption by acid enhanced *Dialium guineense* seed waste. *Arab. J. Sci. Eng.* https://doi.org/10.1007/s13369-020-04771-5 (2020).

81. Sheela, T., Nayaka, Y. A., Viswanatha, R., Basavanna, S. & Venkatesha, T. G. Kinetics and thermodynamics studies on the adsorption of Zn(II), Cd(II) and Hg(II) from aqueous solution using zinc oxide nanoparticles. *Powder Technol.* **217**, 163–170 (2012).

82. Zhang, F., Chen, X., Wu, F. & Ji, Y. High adsorption capability and selectivity of ZnO nanoparticles for dye removal. *Colloids Surf. A Physicochem. Eng. Asp.* **509**, 474–483 (2016).

83. Azizi, S., Mahdavi Shahri, M. & Mohamad, R. Green synthesis of zinc oxide nanoparticles for enhanced adsorption of lead ions from aqueous solutions: Equilibrium, kinetic thermodynamic studies. *Molecules* **22**, 831 (2017).

84. Khosla, E., Kaur, S. & Dave, P. N. Ionic dye adsorption by zinc oxide nanoparticles. *Chem. Ecol.* **31**, 173–185 (2015).

85. Iqbal, M. J. & Ashiq, M. N. Adsorption of dyes from aqueous solutions on activated charcoal. *J. Hazard. Mater.* **139**, 57–66 (2007).

86. Malana, M. A., Ijaz, S. & Ashiq, M. N. Removal of various dyes from aqueous media onto polymeric gels by adsorption process: Their kinetics and thermodynamics. *Desalination* **263**, 249–257 (2010).

87. Dhananasekaran, S., Palanivel, R. & Pappu, S. Adsorption of methylene blue, bromophenol blue, and coomassie brilliant blue by α-chitin nanoparticles. *J. Adv. Res.* **7**, 113–124 (2016).

88. Tambat, S. N., Ahirrao, D. J., Pandit, A. B., Jha, N. & Sontakke, S. M. Hydrothermally synthesized N2-UiO-66 for enhanced and selective adsorption of cationic dyes. *Environ. Technol. Innov.* **19**, 101021 (2020).

89. Mishra, S. R., Chandra, R., Kaila, A. J. & Darshi, B. S. Kinetics and isotherm studies for the adsorption of metal ions onto two soil types. *Environ. Technol. Innov.* **7**, 87–101 (2017).

90. Vishan, I., Saha, B., Sivaprakasam, S. & Kalamdhad, A. Evaluation of Cd(II) biosorption in aqueous solution by using lyophilized biomass of novel bacterial strain *Bacillus badius* AK: Biosorption kinetics, thermodynamics and mechanism. *Environ. Technol. Innov.* **14**, 100323 (2019).

91. Oyewo, O. A., Adeniyi, A., Sithole, B. B. & Onyango, M. S. Sawdust-based cellulose nanocrystals incorporated with ZnO nanoparticles as efficient adsorption media in the removal of methylene blue dye. *ACS Omega* **5**, 18798–18807 (2020).

92. Ma, Y. *et al.* Iron/zinc and phosphoric acid modified sludge biochar as an efficient adsorbent for fluoroquinolones antibiotics removal. *Ecotoxicol. Environ. Saf.* **196**, 110550 (2020).

93. Yan, Y. *et al.* Phosphorus-rich biochar produced through bean-worm skin waste pyrolysis enhances the adsorption of aqueous lead. *Environ. Pollut.* **266**, 115177 (2020).

94. Al-Senani, G. M. & Al-Fawzan, F. F. Adsorption study of heavy metal ions from aqueous solution by nanoparticle of wild herbs. *Egypt. J. Aquat. Res.* **44**, 187–194 (2018).

95. Dong, Y. *et al.* Influence of microwave-assisted synthesis on the structural and textural properties of mesoporous MIL-101(Fe) and NH2-MIL-101(Fe) for enhanced tetracycline adsorption. *Mater. Chem. Phys.* **251**, 123060 (2020).

96. Saffarionpour, S., Tam, S.-Y.S., Van der Wielen, L. A. M., Brouwer, E. & Ottens, M. Influence of ethanol and temperature on adsorption of flavor-active esters on hydrophobic resins. *Sep. Purif. Technol.* **210**, 219–230 (2019).

97. Liang, S., Guo, X., Feng, N. & Tian, Q. Isotherms, kinetics and thermodynamic studies of adsorption of Cu2+ from aqueous solutions by Mg2+/K+ type orange peel adsorbents. *J. Hazard. Mater.* **174**, 756–762 (2010).

98. Ahmad, A. A., Din, A. T. M., Yahaya, N. K. E., Khasri, A. & Ahmad, M. A. Adsorption of basic green 4 onto gasified Glyricidia sepium woodchip based activated carbon: Optimization, characterization, batch and column study. *Arab. J. Chem.* **13**, 6887–6903 (2020).

99. Priyadarshini, B., Behera, S. S., Rath, P. P., Sahoo, T. R. & Parhi, P. K. Adsorption of xylenol orange dye on nano ZnO: Kinetics, thermodynamics and isotherm study. *AIP Conf. Ser.* https://doi.org/10.1063/1.4980276 (2017).

100. Elfeky, A. S., Youssef, H. F. & Elzaref, A. S. Adsorption of Dye From Wastewater onto ZnO nanoparticles-loaded zeolite: Kinetic, thermodynamic and isotherm studies. *Z. Phys. Chem.* **234**, 255–278 (2020).

101. Zhang, M., Chang, L., Zhao, Y. & Yu, Z. Fabrication of zinc oxide/polypyrrole nanocomposites for brilliant green removal from aqueous phase. *Arab. J. Sci. Eng.* **44**, 111–121 (2019).

102. Moritz, M. & Geszke-Moritz, M. The newest achievements in synthesis, immobilization and practical applications of antibacterial nanoparticles. *Chem. Eng. J.* **228**, 596–613 (2013).

103. Rai, M., Yadav, A. & Gade, A. Silver nanoparticles as a new generation of antimicrobials. *Biotechnol. Adv.* **27**, 76–83 (2009).

104. Savi, G. D., Bortoluzzi, A. J. & Scussel, V. M. Antifungal properties of Zinc-compounds against toxigenic fungi and mycotoxin. *Int. J. Food Sci. Technol.* **48**, 1834–1840 (2013).

Acknowledgements

Author contributions

K.G.A. and S.G., conceptualized the research, conducted laboratory experiments, analyzed the obtained data and wrote the manuscript. M.G. and J.C. supervised, read and edited the manuscript and provided financial support to conduct the research.

Competing interests

The authors declare no competing interests.

Additional information

Supplementary Information The online version contains supplementary material available at https://doi.org/10.1038/s41598-021-87819-2.

Correspondence and requests for materials should be addressed to K.G.A.

Reprints and permissions information is available at www.nature.com/reprints.

Publisher's note Springer Nature remains neutral with regard to jurisdictional claims in published maps and institutional affiliations.